Conformational Changes of α-Chymotrypsin in a Fibrillation-Promoting Condition: A Molecular Dynamics Study

Nasrollah Rezaei-Ghaleh,* Mehriar Amininasab,† and Mohsen Nemat-Gorgani*‡
*Institute of Biochemistry and Biophysics, †Department of Cell and Molecular Biology, Faculty of Science, University of Tehran, Tehran, Iran; and ‡Stanford Genome Technology Center, Stanford University, Palo Alto, California

ABSTRACT Amyloid nanofibril formation appears to be a generic property of polypeptide chains. α-Chymotrypsin (aCT) was recently driven toward amyloid-like aggregation by the addition of trifluoroethanol (TFE) at intermediate concentrations. In this study we employed a molecular dynamics simulation to investigate the early events in TFE-induced conformational changes of aCT that precede amyloid formation, and compared the results of the simulation with previous experiments. TFE molecules were found to rapidly replace the water molecules closely associated with the protein surface. The gyration radius, together with total and hydrophobic solvent-accessible surface areas of aCT, was significantly increased. In accord with the experimental observations, the extended β-conformation of backbone was increased. The secondary structural elements of aCT in water and TFE/water mixture showed a reasonable fit, whereas significant deviations were observed for several loops. These alterations originated largely from main-chain rotations at glycine residues. The catalytic active site and S1 binding pocket of the enzyme were also distorted in the TFE/water mixture. The obtained results are suggested to provide more insights into the conformational properties of the amyloid aggregation-prone protein species. Possible mechanisms of TFE-induced alterations in the conformation and dynamics of the protein structure are also discussed.

INTRODUCTION

The effects of alcohols on the structure of peptides and proteins have been studied extensively over the last few decades (1–4). It has been shown that various alcohols denature the native state of proteins and stabilize the α-helical structures (4–6). 2,2,2,Trifluoroethanol (TFE) is known for its marked ability in this regard (7). TFE has been demonstrated to induce and stabilize α-helical conformations in peptides and proteins, in good correlation with the intrinsic α-helical propensities of their primary sequences (8). It has also been reported to induce β-turns, β-hairpins, β-strands and sheets, and hydrophobic clusters (5,7,9–11). At high TFE concentrations, proteins are known to adopt the so-called TFE- or T-state conformation, which is characterized by a larger size and greater flexibility than the native state, a disrupted hydrophobic core, and a richer α-helical content (12). Some proteins may exhibit an aggregation-prone molten globule state at low TFE concentrations before they reach the final T state (12). Conformational changes affected by TFE appear to depend on the particular amino acid sequences, the cosolvent concentration, and other solution conditions and protein structures (7).

Although the effects of TFE on proteins have been known for a long time, the physical mechanisms by which TFE and related cosolvents affect polypeptide chain conformations are still unclear. The lower dielectric coefficient of alcohol/water mixtures with respect to pure water may weaken hydrophobic interactions within the protein molecule and simultaneously enhance local electrostatic interactions, including hydrogen bonds, within the protein secondary structures (13,14). The more remarkable effect of fluorine-substituted alcohols, including trifluoroethanol, has been attributed to the formation of large clusters of alcohol molecules within the alcohol/water mixtures, which may provide proteins with high local alcohol concentrations (15). The hydrophobic character of the $-CF_3$ group may be a major factor responsible for cluster formation, which occurs maximally around 30% TFE (15,16). In addition, the strong electron-withdrawing effect of fluorine atoms makes TFE a better proton or hydrogen bond donor, but a poorer acceptor, compared to water (7). It has been suggested that such a preferential interaction may lead to enhanced intrapolypeptide hydrogen bonding of the amide group as solvent exposure of the amide is minimized (17,18). The stabilizing effects of TFE on helical conformations were alternatively suggested to be caused by destabilization of backbone exposure either due to its kosmotropic effect and resultant desolvation (19,20), or its lower polar characteristic and selective destabilization of the planar resonance-stabilized amides (21). The preferential accumulation of fluorinated alcohol molecules around peptide and protein surfaces, as suggested by experimental and simulation findings, is expected to displace water, thereby removing alternative hydrogen-bonding partners and providing a low dielectric environment that favors formation of intrapeptide hydrogen bonds (22–29). Some authors have suggested that the folded

Submitted February 26, 2008, and accepted for publication July 7, 2008.

Address reprint requests to Mehriar Amininasab, Tel.: 98-21-6111-3314; Fax: 98-21 6649-2992; E-mail: amininasab@khayam.ut.ac.ir; or to Mohsen Nemat-Gorgani, Tel.: 650-812-1961; Fax: 650-812-1975; E-mail: mohsenn@stanford.edu.

Nasrollah Rezaei-Ghaleh's present address is Dept. of NMR-Based Structural Biology, Max-Planck-Institute for Biophysical Chemistry, Goettingen, Germany.

Editor: Ron Elber.

0006-3495/08/11/4139/09 $2.00

doi: 10.1529/biophysj.108.132407

state (e.g., the helix state) is preferentially solvated by TFE, leading to its stabilization relative to the coil state (30,31).

Amyloid nanofibrils are straight and unbranched, usually 5–14 nm in diameter and several hundred nanometers in length, and show a characteristic cross-β pattern in x-ray diffraction studies (32). Several types of human diseases, including Alzheimer's, Parkinson's, and Huntington's diseases, and bovine spongiform encephalopathy, are known to be associated with amyloidogenesis (33). Because of vast clinical importance, there is now a strong motivation to investigate more closely the issue of amyloid aggregation, i.e., to characterize the initial aggregation-prone state of the polypeptide chains and its final morphology, and to elucidate the mechanisms involved. Although remarkable advances have been made, many aspects of protein misfolding leading to amyloid nanofibril formation remain unclear (34). It is widely believed that partially (un)folded molten globule-like protein structures are especially susceptible to amyloid aggregation (35–37). Computational approaches have also provided useful molecular pictures of amyloid structure and formation (35, 38–40).

There exists an abundant amount of evidence suggesting that amyloid nanofibril formation is not restricted to a limited number of clinically important proteins, but is a generic property of polypeptide chains (41). It was recently demonstrated that α-chymotrypsin, a well-known serine protease with an all-β fold, could be driven toward amyloid aggregation by the addition of TFE at intermediate concentrations (42). α-Chymotrypsin is a three-chain protein connected by five inter- and intrachain disulfide bonds. This protein is folded into two antiparallel β-barrel domains consisting of a Greek key motif followed by an antiparallel hairpin motif (43). In this study we used a molecular dynamics (MD) simulation to investigate the early events in TFE-induced conformational changes of α-chymotrypsin that precede the initial phases of its amyloid fibrillation. It is suggested that the resulting information may provide better insights into the structural properties of the amyloid aggregation-prone species.

MATERIALS AND METHODS

The crystal structure of bovine α-chymotrypsin at 1.68 Å resolution (with Protein Data Bank identification code of 4CHA) (44) was used to model unliganded α-chymotrypsin. Two missing residues in 4CHA (residues 12–13) were added by taking their coordinates from the crystal structure of bovine α-chymotrypsin in complex with eglin (with identification code of 1ACB) (45) after removal of the ligand and fitting of two structures over the backbone atoms. Then the protein was solvated with either pure water or a preequilibrated mixture of TFE and water (with TFE v/v concentration of ~30%) and placed in a periodic cubic box with 6.95-nm-long edges. The protonation state of the protein molecule at pH 7.0 was calculated after estimating the pKa of titratable groups by the H++ server (accessible at http://biophysics.cs.vt.edu/H++/). One of the two existing histidines (His^{40}) was considered to be uncharged with the hydrogen atom bound to NE2, and Glu^{70} was regarded as an uncharged residue. To neutralize 21 positive and 16 negative charges on the protein molecule, 37 water molecules were replaced with counterions (21 Cl^- and 16 Na^+, respectively). In all of the simulation runs, temperature and pressure were kept close to the intended values (300 K and 1 bar) by using the Berendsen algorithm (46) with $\tau_T = 0.1$ and $\tau_P = 0.5$ ps, respectively. Before starting the MD simulations, the energy of each system was minimized using a steepest-descent algorithm.

All MD simulations and analyses of the resultant trajectories were performed using the GROMACS 3.2 simulation package (47) with the GROMOS96 force field (48). The simple point charge (SPC) water model (49) was used together with a previously optimized TFE model (50). The LINCS algorithm was used to constrain all bond lengths in the protein and TFE molecules (51). A single-range cutoff was used for calculation of the nonbonded interactions. The cutoff radius was set to 1.2 nm for both Coulombic and Lennard-Jones interactions. The Coulombic interactions of longer range were calculated by means of the particle-mesh Ewald (PME) algorithm (52). All atoms were given an initial velocity obtained from a Maxwellian distribution at the desired initial temperature. Simulations were equilibrated by 100 ps of MD with position restraints on the protein to allow for relaxation of solvent molecules. These first equilibration runs were followed by another 100-ps runs without position restraints on the protein. The production periods after equilibration in pure water and the TFE/water mixture were 5 and 35 ns long, respectively. Time steps of 2 fs duration were used and frames were collected at 250-step intervals, i.e., with intervals of 0.5 ps.

The local concentration (v/v percent) of TFE and water (LTC and LWC, respectively) in the vicinity of the protein surface were evaluated from the number of solvent and cosolvent molecules present in a shell of 0.6 nm around the protein surface. LTC and LWC were calculated separately for various residues through enumeration of TFE and water molecules in a sphere of 0.9 nm radius around their centers of mass. Average excluded volume values of 0.019 and 0.07 $L \cdot mol^{-1}$ were assumed for water and TFE, respectively (28). Supposing a first-order kinetic for solvation and desolvation processes, $LTC_{(t)}$ was fitted to the following equation:

$$(LTC_{(t)} - LTC_{(eq)})/(LTC_{(0)} - LTC_{(eq)}) = e^{-kt},$$

where $LTC_{(0)}$ is the value of LTC at the first frame of simulation, and $LTC_{(eq)}$ is its limiting value. Since solvation and desolvation processes occur simultaneously, the rate constant k is actually the sum of rate constants for solvation by TFE (k_{sol}) and desolvation (k_{des}). Since $k_{sol}/k_{des} = LTC_{(eq)}/BTC$, where BTC is the bulk TFE concentration, separate k_{sol} and k_{des} could be simply derived. The mean residence time of TFE molecules over the protein surface was estimated as $1/k_{des}$. A similar analysis was made independently for LWC.

Cluster analysis was performed using the linkage method and a cutoff root mean-square deviation (RMSD) of 0.1 nm. The RMS calculations were made at 250-ps intervals. The graphical images were produced by means of the VMD 1.8.6 program (53).

RESULTS AND DISCUSSION

α-Chymotrypsin was recently driven toward amyloid aggregation using a ~30% v/v concentration of TFE (42,54). Based on a variety of spectroscopic techniques, it has been suggested that the amyloid aggregation-prone state of α-chymotrypsin is a partially unfolded structure with molten globule-like features (42). In the study presented here, we employed an MD simulation technique to characterize the early events related to TFE-induced structural and dynamic changes of α-chymotrypsin, and compared the results with those obtained from previous experiments (42,54,55).

Fig. S1 in Supplementary Material, Data S1, displays the temporal variation of the potential energy of α-chymotrypsin in the TFE/water mixture along the 35-ns trajectory. The decreasing trend of fluctuating potential energy evidently

reached its equilibrium value of approximately −259.4 (±0.5) MJ·mol^{-1} after 5 ns. Accordingly, the trajectory produced after 5 ns was considered as a sample of the equilibrated NPT ensemble of α-chymotrypsin in 30% TFE, and the statistical analyses were then restricted to this period of simulation. In water, the average potential energy remained nearly constant at −482.5 (±0.5) MJ·mol^{-1} along the whole 5 ns of the simulated trajectory (Fig. S1 in Data S1).

Effects of TFE on protein solvation

To see how TFE molecules behave along the simulation trajectory, the radial distribution function (RDF) of TFE was calculated at various time steps. As depicted in Fig. 1 *A*, TFE molecules gradually accumulated over the protein surface, so that after 1 ns the RDF of TFE revealed a clear peak around 2.25 nm away from the mass center of the α-chymotrypsin molecule. During the remainder of the simulation process, the RDF of TFE did not change considerably except that at the end, small peaks were developed at $r = 0.65$, 0.78, and 1.06 nm, indicating that some TFE molecules must have penetrated into the core of the protein structure. The calculated RDF revealed that water molecules were soon displaced from the vicinity of the protein molecule during the simulation (Fig. S2 in Data S1). Since the calculated radius of α-chymotrypsin in the TFE/water mixture is ~2.14 nm (see below), the fact that the RDF of TFE peaked at 2.25 nm indicates that the shell of TFE molecules is closely located around the protein surface. Fig. 1 *B* illustrates four snapshots of the TFE-coated chymotrypsin molecule at the end of simulation. Obviously, most surface regions are extensively occupied by TFE, although there are also some residues on the protein surface that seem to be relatively less solvated by TFE. A closer inspection revealed that residues 1, 5–7, 36, 61–63, 76–78, 92–97, 146, 186–187, 204–205, 218–224, and 243–244 were more exposed to water than the average (see below for further analysis).

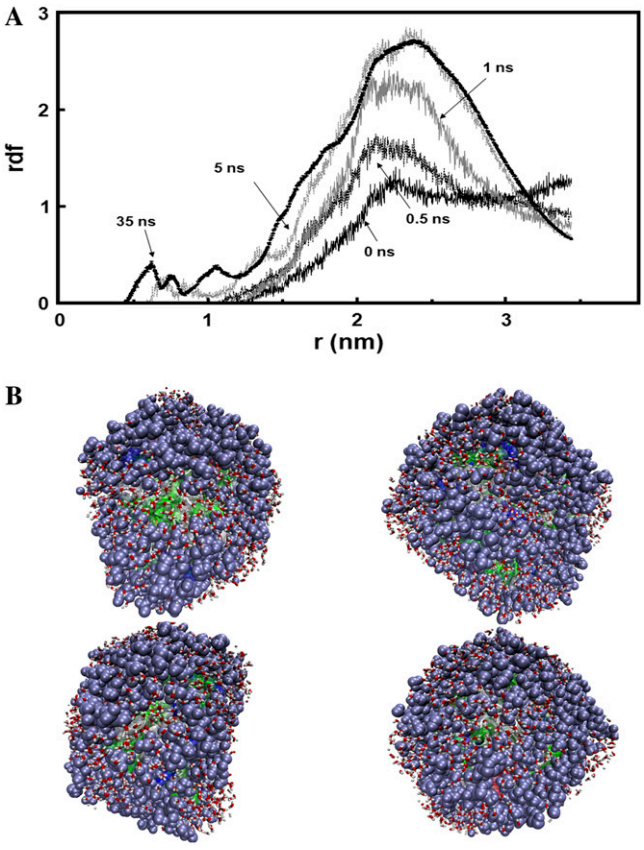

FIGURE 1 (*A*) RDF of TFE at various times in the 35-ns MD simulation. (*B*) Four snapshots of a TFE-coated α-chymotrypsin molecule at the end of the 35-ns-long simulation in TFE/water mixture.

The kinetics of protein solvation was studied by monitoring temporal changes of local TFE and water v/v concentrations (LTC and LWC, respectively) along the simulation. As demonstrated in Fig. 2, the LTC rises exponentially to a final value of ~85%, whereas the LWC decays in a similar manner to 15%. The solvation and desolvation rate constants (k_{sol} and k_{des}, respectively) were 8.433×10^8 and 2.925×10^8 s^{-1} for TFE, and 2.014×10^8 and 9.347×10^8 s^{-1} for water. The average residence time of TFE in the protein surface was 3.4 ns. The apparent binding constant for TFE ($LTC_{(eq)}$/BTC) was 2.883, in accord with several simulation reports (24,28) and as experimentally estimated for β-lactoglobulin (25).

MD simulations have revealed that TFE molecules preferentially aggregate around peptides with different secondary structural characteristics (24,28). The preferential presence of fluorinated alcohol molecules in the vicinity of peptide and protein molecules, and the simultaneous exclusion of water molecules have also been experimentally verified by several experimental approaches, including intermolecular nuclear Overhauser effect (NOE) and nuclear magnetic resonance dispersion (NMRD) studies (23–27). An NMRD study has demonstrated that several hundred moderately perturbed TFE molecules coat a similar protein (β-lactoglobulin) at 21% TFE, whereas some TFE molecules are entrapped in the protein core and reside there for a sufficiently long time to give rise to an observable frequency dependence of longitudinal

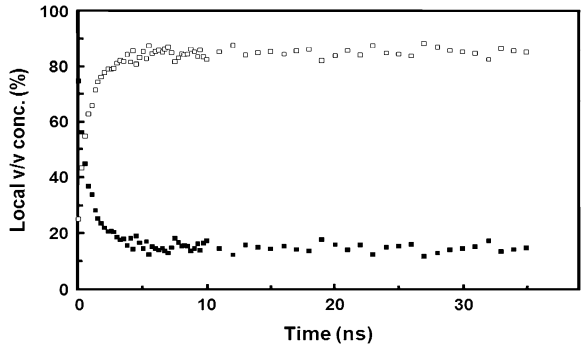

FIGURE 2 Time-dependent alteration of local TFE (□) and water (■) v/v concentration around the protein surface.

relaxation rates R_1 of fluorine nuclei (25). In agreement with these experimental and simulation reports, our results suggest that several hundred TFE molecules accumulate over the chymotrypsin surface and some of them penetrate into the protein core, whereas water molecules are displaced from the protein surface. As suggested earlier (28,29), the coating of protein surface by TFE and the concomitant detachment of water molecules remove alternative hydrogen-bonding partners and provide a very low dielectric environment that favors the formation of local hydrogen bonds (14). In addition, this TFE-rich local environment can significantly weaken hydrophobic interactions, thereby promoting dislocation of hydrophobic residues toward protein surface. The estimated residence time of TFE molecules within the 0.6-nm-thick shell around the protein surface is 3.4 ns, which is ~34-fold longer than the time required for TFE molecules to diffuse over that distance. This indicates a remarkable interaction of TFE molecules with the protein surface that prevents them from returning to the bulk solution. The TFE residence time, however, is shorter than the rotational correlation time of ~22 ns when the experimentally observed value of 12 ns for native α-chymotrypsin is corrected for the viscosity of TFE/water mixture (56).

To explore which parts of the protein surface are preferentially coated by TFE molecules, the LTC was calculated around different residues of the protein (Fig. 3). The mean ± SD of LTC was 81.2 ± 15.1. Obviously, the LTC around all the residues was considerably higher than the bulk TFE concentration, except for Ser^{45}, Val^{52}, Val^{53}, Ser^{189}, Gly^{226}, and Tyr^{228}. A weak correlation coefficient (−0.093) was found between the Kyte hydropathic index of amino acid residues (57) and their LTCs. The negative sign of correlation indicated that, in general, higher LTCs were observed around more hydrophilic residues. The charged residues also showed slightly higher LTCs (85.4 ± 6.5). No significant difference in LTC was found between aromatic and nonaromatic residues or between residues of various secondary structures. When the tertiary structure of the protein was examined in terms of TFE-induced solvent-accessible surface area (SASA) changes, a positive correlation coefficient of 0.19 was observed, indicating that the residues with greater positive SASA change generally manifest higher LTCs. Indeed, the six residues with LTC lower than the bulk were found to be significantly more buried in the TFE-induced conformation than the native state. Altogether, our results suggest that TFE accumulation on the protein surface is a rather global phenomenon, although some differences exist among residues of various side-chain properties. Furthermore, it appears that the intrinsic propensity of TFE toward various residues may be masked by the global structural changes of a large protein, so that the residues that are moved toward the interior of the protein cannot be solvated well by TFE.

Effects of TFE on protein size and surface properties

TFE-induced alterations in native conformations of proteins are expected to cause an increase in their size, as a result of protein unfolding. Fig. 4 illustrates how the gyration radius of α-chymotrypsin was varied along the simulation trajectory in the TFE/water mixture. In water, the gyration radius of α-chymotrypsin revealed obvious fluctuations around an average value of 1.63 ± 0.01 nm. For the protein molecule at 30% TFE, the gyration radius manifested a clear rising trend, so that the average value of gyration radius was 1.66 ± 0.01 nm during the last 10 ns of the simulation trajectory. Assuming a spherical shape for the protein molecule, the radius of α-chymotrypsin molecule in water and the TFE/water mixture was estimated as 2.10 and 2.14 nm, respectively. This means a rise of ~6% in the volume of the α-chymotrypsin molecule. Enlargement of the protein molecule and accumulation of relatively tightly bound TFE molecules over its surface must lead to a more pronounced increase in its hydrodynamic radius (24). The simulated TFE-induced enlargement of the α-chymotrypsin molecule is consistent with earlier experimental measurements on the molecular size of other proteins (hen egg-white lysozyme and α-lactalbumin) (12,58).

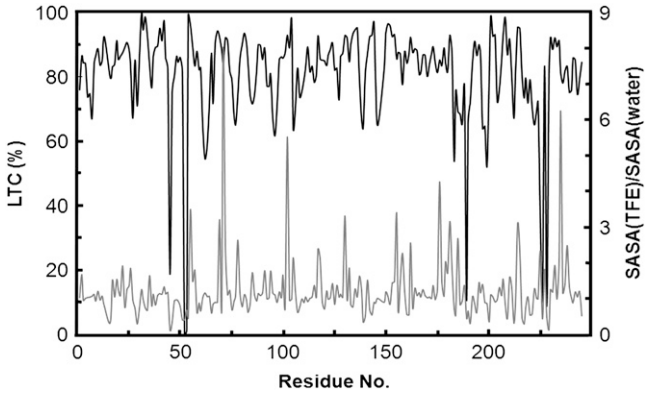

FIGURE 3 Variation of LTC around different residues of α-chymotrypsin. The lower graph displays the ratio of SASA in TFE/water mixture to SASA in water for the same residues.

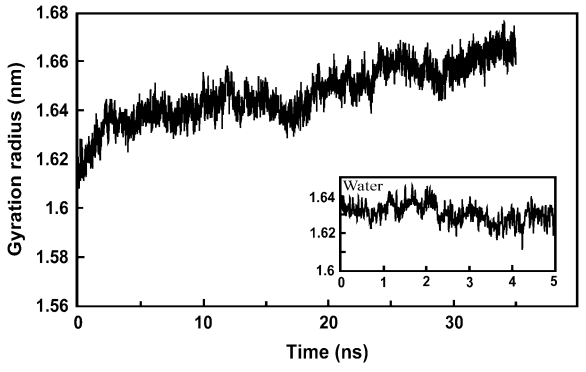

FIGURE 4 Temporal changes of α-chymotrypsin gyration radius during the 35-ns MD simulation in TFE/water mixture. The inset shows how the gyration radius varied along the 5-ns simulation in water.

Alcohols are widely believed to cause significant changes in the properties of protein surfaces, and hence alcohol-induced products may become prone to associate intermolecularly. To investigate this event, the total and hydrophobic SASAs of α-chymotrypsin were calculated as a function of time (Fig. 5). For α-chymotrypsin simulated in water, the total and hydrophobic SASAs fluctuated around average values of 110.3 $\pm$ 1.9 and 61.4 $\pm$ 1.6 nm^2, respectively. In the TFE/water mixture, the total SASA of α-chymotrypsin was increased throughout the simulation process and larger hydrophobic patches were exposed over its surface. The average values of total and hydrophobic SASA were 120.1 $\pm$ 3.1 and 67.8 $\pm$ 2.0 nm^2, respectively, between 5 and 35 ns. This is in accord with previous reports of enhanced 1-ani-1-anilino-8-naphthalene sulfonate (ANS) emission, which indicate that in TFE/water mixtures, larger hydrophobic patches are exposed over the α-chymotrypsin surface (42). Fig. S3 in Data S1 depicts the solvent-exposed hydrophobic surface of the initial and final structure of α-chymotrypsin as simulated in the TFE/water mixture. Exposure of hydrophobic patches over the surface of α-chymotrypsin may contribute positively to its susceptibility to aggregation (42,54).

The greatest positive changes in total SASA were observed for Phe^{130}, Glu^{78}, His^{57}, Trp^{215}, and Tyr^{94}, followed by Ala^{132}, Lys^{177}, Arg^{154}, Asp^{72}, and Ala^{185}. Residues with significant positive changes in SASA (above 0.1 nm^2) showed less hydrophobic character than the average of the protein (i.e., lower hydropathic indices in the Kyte and Doolittle scale (57)). It was also found, surprisingly, that eight of the nine Asp residues of the protein were more solvent-exposed in the TFE-induced structure. This unexpected finding may be attributed to a greater tendency of TFE to form H-bonds as a donor than as an acceptor (7,17), so that in the vicinity of TFE, residues with complementary H-bonding capability (such as the Asp side chain, which is a strong H-acceptor) may tend to move toward the surface.

The TFE-induced drop in the fluorescence emission intensity of α-chymotrypsin, together with a marked red shift in its emission spectrum, is likely to be caused by the greater solvent accessibility of the responsible aromatic residues,

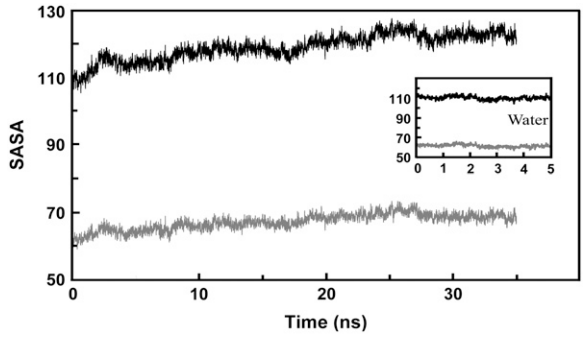

FIGURE 5 Time-dependent alteration of total (*black*) and hydrophobic (*gray*) SASAs of α-chymotrypsin during the 35-ns MD simulation in TFE/water mixture and the 5-ns simulation in water (*inset*). The unit of area is nm^2.

including the eight tryptophans of α-chymotrypsin that are highly buried in the native state (42,55). The significant loss of near-UV CD signal around 289 nm was also explained in a similar manner (42). In accord with this proposed mechanism, the results of our MD simulation indicate that tryptophans 141, 207, 215, and 237 of α-chymotrypsin were considerably more exposed in the TFE/water mixture than in pure water (52%, 56%, 132%, and 41% increases in SASA, respectively). The total SASA of eight tryptophan residues also revealed an increase of ~30%. Similar results were obtained for the four tyrosine and six phenylalanine residues of α-chymotrypsin (data not shown).

Tryptophans 207 and 215, which were significantly exposed to the solvent in the TFE-induced structure of α-chymotrypsin, are located within the β-strand 206–215 (AWTLVGIVSW), which is rich in hydrophobic and aromatic residues and devoid of any charge. π-Stacking between aromatic residues is widely believed to provide an additional stabilizing effect on intermolecular β-sheets of the amyloids (59). Furthermore, the use of the PASTA algorithm shows that this fragment has a high tendency to adopt parallel in-register β-strand alignment within the ordered self-propagating cross-β structure of the formed amyloids (60). Taken together, the above points suggest that fragment 206–215 may later be involved in formation of the cross-β core structure of the amyloids.

Effects of TFE on protein structure

TFE is known for its marked ability to stabilize and/or induce secondary structures in peptides and proteins (7). Various types of secondary structures may be induced by this fluorinated alcohol (5,7–11). It was recently suggested that TFE at ~30% concentration increases the extended β-strand conformation in α-chymotrypsin (42,54,55). Accordingly, the simulated ensemble of α-chymotrypsin molecules in the TFE/water mixture showed a slight change in secondary structure with respect to the initial form. These changes favored the extended β-strand conformation, so that the number of residues with this conformation increased from 69 $\pm$ 4 in water to 75 $\pm$ 4 in the TFE/water mixture. The new residues that adopted an extended β-strand conformation were Gln^{30}, Val^{31} and Ser^{32}, Gly^{43} and Gly^{44}, Ile^{47} and Asn^{48}, Ala^{55}, Val^{65}, Ile^{103}, Gly^{133} and Thr^{134}, and Arg^{230} located at the N- and C-terminal sides of the native β-strands, suggesting that TFE promoted the extension of existing β-strands. On the other hand, the number of residues with coil or bend structures showed a slight decrease. In regard to the number of hydrogen bonds, the total number of backbone H-bonds decreased from 163 in water to 151 in the TFE/water mixture. The most significant changes occurred in the number of H-bonds between O(I) and H-N(I + 2), which decreased from 45 in water to 32 in the TFE/water mixture, and the number of H-bonds in antiparallel β-sheets, which increased from 65 to 74. All of these secondary structural transitions can be taken to suggest that TFE induces more extended structures

as compared to the native state. The formation of such extended conformational states may constitute the early events related to the TFE-induced amyloid aggregation-prone state, as suggested by a previously reported MD simulation study (34). The proposed native-like secondary structural features combined with partial loss of the native tertiary structure is consistent with earlier suggestions that the amyloid aggregation-prone state of α-chymotrypsin induced at 30% TFE shows molten globule-like properties (42,54).

In Fig. 6, the RMSD with respect to the initial crystal structure is reported for α-chymotrypsin in the TFE/water mixture as a function of time. In water, the RMSD of the backbone atoms of α-chymotrypsin showed a sharp rise in the first nanosecond followed by a slight increase during the rest of the simulation process, so that at the end of the 5-ns simulation, it reached a value of ~0.18 nm. In the TFE/water mixture, most changes in the RMSD occurred during the first 5 ns. During the subsequent 30 ns, the RMSD revealed a slow rise to 0.21 nm. When the backbone RMSD in the TFE/water mixture of various residues was plotted against their RMSD in water, several residues were found with significantly different RMSD values in water and the TFE/water mixture (Fig. S4 in Data S1). The observed increase in the RMSD value in water was prominently caused by residues 11–13 (C-terminal of A-chain), 115–117, 126–133; the autolysis loop: 145–146 (C-terminal of B-chain) and 149–152 (N-terminal of C-chain); the methionine loop: 170–175; and the S1 binding pocket: 191–194, 217–221, and 244–245 (C-terminal of C-chain). However, in TFE/water mixtures, residues 60–64, 73–79, 91–98, 127–133, 144–146 (C-terminal of B-chain), 149–150 (N-terminal of C-chain), 174–178, 186–189, 203–206, and 214–224 had the most significant contributions (Fig. 7).

Fig. 8 compares the average structure of α-chymotrypsin in the TFE/water mixture with that obtained in water. The RMSD of the backbone atoms of α-chymotrypsin was 0.2 nm. Although the secondary structure elements of α-chymotrypsin were well fitted, the loops manifested considerable deviations between the two structures. The most significant

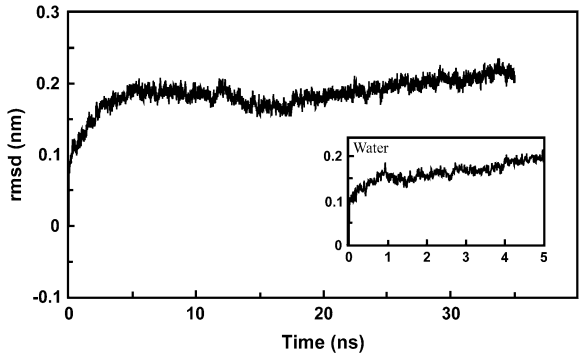

FIGURE 6 Changes in the RMSD for the backbone atoms of α-chymotrypsin during the 35-ns MD simulation in TFE/water mixture and the 5-ns simulation in water (*inset*).

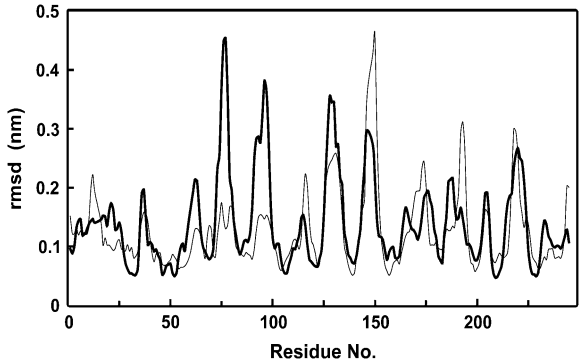

FIGURE 7 Backbone RMSD of α-chymotrypsin, calculated per residue with respect to the initial structure as the average over the simulated trajectory in water (*thin line*) and TFE/water mixture (*thick line*).

deviations were observed in regions Asp^{35}-Phe^{39}, His^{57}-Asp^{64}, Gly^{74}-Lys^{79}, Ser^{92}-Asn^{101}, Ala^{126}-Thr^{134}, the autolysis loop (C-terminal of B- and N-terminal of C-chains), and Met^{186}-Ser^{195} (the S1 binding pocket; see also Fig. 7). For loop 36-38, the deviation was caused by significant rotations of the polypeptide backbone around C_α-C of Asp^{35} and N-C_α of Lys^{36}. These in turn resulted in a peaked displacement of Thr^{37}, whereas the backbone conformation of Thr^{37} (its backbone dihedrals) was relatively unchanged. On the other side, the backbone conformational change of Gly^{38} and Phe^{39} returned the main polypeptide chain to its initial direction. A significant deviation of Thr^{61}, Thr^{62}, and Ser^{63} was similarly caused by main-chain rotations around residues His^{57}, Cys^{58}, and Gly^{59}. In the case of loop Gly^{74}-Lys^{79}, the most significant displacements were observed for Ser^{76} and Ser^{77}, resulting from the main-chain rotations at Gly^{74}, Ser^{76}, and Lys^{79}. For the loop Ser^{92}-Asn^{101}, the largest rotations occurred at Ser^{92}, Lys^{93}, Tyr^{94}, and Ile^{99}, and maximal displacement appeared at Ser^{96}. The backbone deviation observed between Ser^{127} and Thr^{134} (with peaks at Asp^{128} and Asp^{129}) also originated from main-chain rotations at Ser^{127}, Gly^{133}, and Thr^{134}. Another obvious deviation, observed at Asp^{192} and Ser^{193} of the S1 binding pocket, originated from main-chain rotations at Met^{188}, Gly^{189}, and Gly^{194}. Considering these findings, it appears that some of the pivotal points of the largest main-chain rotations responsible for TFE-induced conformational changes of α-chymotrypsin are glycine residues. This is consistent with a proposed role of glycine residues as hinges during the activation of the enzyme precursor (43).

The catalytic triad of the enzyme—Ser^{195}, His^{57}, and Asp^{102}—was also found to be significantly distorted in the TFE/water mixture (Fig. 8 *B*). All of these three residues showed a higher than average degree of solvation by TFE (with LTCs of 90%, 84%, and 93%, respectively). The side-chain conformation of His^{57} changed from *gauche*+ to *gauche*−, orienting its imidazole ring away from the Ser^{195} hydroxyl group. Fig. 9 illustrates how the distance between the critical residues Ser^{195} and His^{57} varies throughout the simulated trajectories. Although the final distance in water

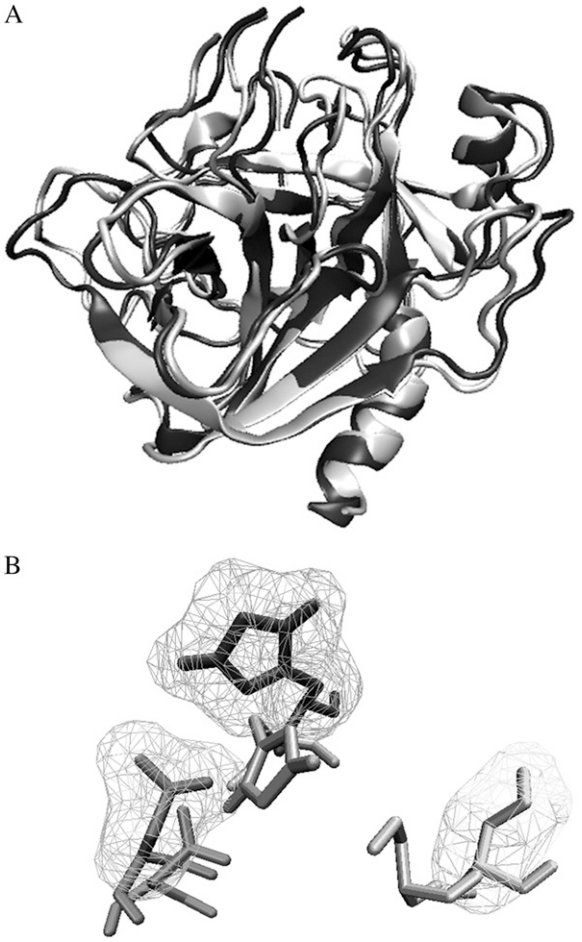

FIGURE 8 (*A*) Ribbon representation of the average structures of α-chymotrypsin in water (*light gray*) and TFE/water mixture (*dark gray*) after fitting. (*B*) Average structure of the catalytic triad (Ser^{195}, His^{57}, and Asp^{102}) of α-chymotrypsin in water (bare) and TFE/water mixture (covered by wire frames).

was nearly identical to the initial value (despite some large fluctuations in the first 2 ns of simulation), the interresidue gap significantly widened during 10–20 ns of the simulation run at 30% TFE, so that the final distance in TFE/water mixture was about three times that in water. Relatively similar TFE-induced changes were observed for two other interresidue distances within the catalytic triad (data not shown). Since the right distance and orientation of these residues are crucial for the enzymatic activity of α-chymotrypsin, the TFE-induced changes in the active site structure of α-chymotrypsin seem likely to result in a prominent loss of enzymatic function. This is consistent with the previous experimental reports of TFE-induced activity loss (54,55).

Formation of a salt bridge between the α-amino group of Ile^{16} (the N-terminal amino group of the B-chain) and side-chain carboxyl of Asp^{194} is known to be a critical event that would initiate a cascade of conformational changes and finally lead to formation of substrate binding site S1 and activation of α-chymotrypsin. The Ile^{16}-Asp^{194} distance was shown to decrease prominently in the TFE/water mixture, suggesting a strengthening of this salt bridge. Such strengthening may have been caused by the lower dielectric coefficient of the medium resulting from the presence of TFE.

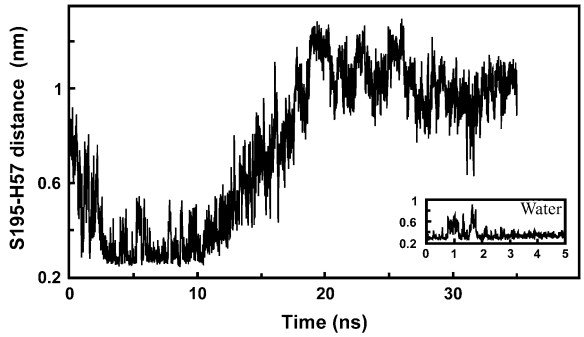

FIGURE 9 Temporal variation of the distance between Ser^{195} and His^{57} during the 35-ns MD simulation in TFE/water mixture and the 5-ns simulation in water (*inset*).

Effects of TFE on protein backbone dynamics

The enzymatic activity of α-chymotrypsin is known to be influenced by protein dynamics. Motions in proteins are governed in part by electrostatic interactions (61). Stronger electrostatic interactions as a result of a lower dielectric constant should thus have a major effect on protein dynamics. Electron paramagnetic resonance (EPR) spectroscopy and MD calculations verified that, at lower dielectric constants, many atoms of α-chymotrypsin move more slowly, and many of the slowest moving residues are near the exterior (62). As indicated by the calculated RMS fluctuation (RMSF) of the backbone atoms in water and the TFE/water mixture, the flexibility of the polypeptide chain appears to change variably in different regions of α-chymotrypsin. Although residues 35–39, 190–194, and 216–220 moved more slowly in the TFE/water mixture than in pure water, residues 74–79 and 91–98 were significantly more flexible (Fig. 10). It is also

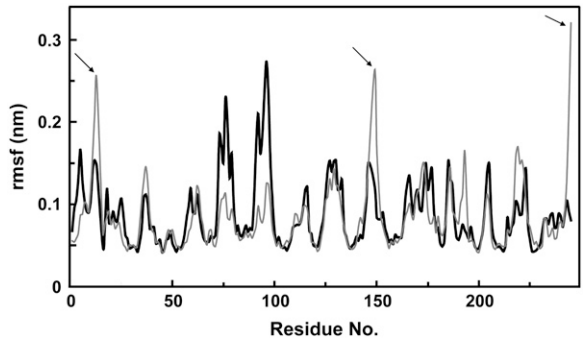

FIGURE 10 RMSF of backbone atoms, calculated per residue with respect to the average structure of α-chymotrypsin simulated in water (*thin line*) and TFE/water mixture (*thick line*). The arrows point to the N- and C-termini of the polypeptide chains (*A–C*) with diminished flexibility.

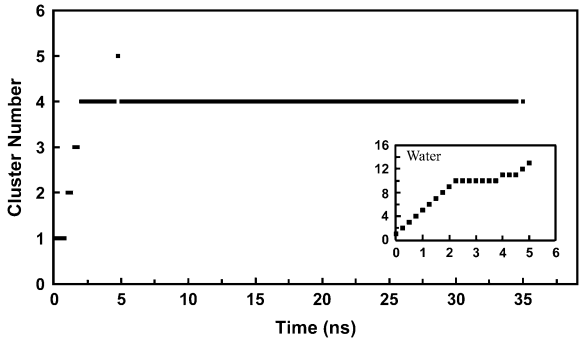

FIGURE 11 Time course of the different clusters of structures obtained during the 35-ns MD simulation in TFE/water mixture and the 5-ns simulation in water (*inset*).

obvious that the polypeptide N- and C-terminal ends, which are near the exterior of the protein, become more rigid in the TFE/water mixture. On the other hand, His^{57} of the catalytic triad manifested a significant increase in flexibility.

To investigate the conformational diversity in the TFE/water mixture, a clustering analysis of the simulated trajectories was performed. As demonstrated in Fig. 11, 13 distinct clusters appeared along the 5-ns-long trajectory in water, with the largest cluster representing 35% of the trajectory. On the other hand, only five clusters were obtained in the 35-ns-long simulated trajectory in the TFE/water mixture, with the largest one representing ~95% of the trajectory. The smaller number of clusters in the TFE simulation indicates a lower conformational diversity in the TFE/water mixture. This is in good agreement with experimental and simulation evidence of diminished conformational diversity in fluorinated alcohols (29,62).

In conclusion, we employed a 35-ns-long MD simulation to follow the earliest TFE-induced alterations in the conformation and dynamics of α-chymotrypsin that precede the amyloid-like fibrillation of this protein. The obtained results, indicating a significant TFE-induced rise in the gyration radius and total and hydrophobic SASA of the protein, in addition to the accumulation of TFE over the protein molecule, the higher extended-β conformation, molten-globule-like features of the TFE-induced α-chymotrypsin species, distortion of the catalytic active site and S1 binding pocket, and changes in the backbone flexibility, were all in reasonable agreement with previous reports. The obtained results may shed some more light on the possible mechanisms of TFE effects and conformational properties of the TFE-induced amyloidogenic protein species.

SUPPLEMENTARY MATERIALS

To view all of the supplemental files associated with this article, visit www.biophysj.org.

This work was supported by a grant from the Research Council of the University of Tehran.

REFERENCES

1. Schrier, E. E., R. T. Ingwall, and H. A. Scheraga. 1965. The effect of aqueous alcohol solutions on the thermal transition of ribonuclease. *J. Phys. Chem.* 69:298–303.
2. Parodi, R. M., E. Bianchi, and A. Ciferri. 1973. Thermodynamics of unfolding of lysozyme in aqueous alcohol solutions. *J. Biol. Chem.* 248:4047–4051.
3. Fink, A. L., and B. Painter. 1987. Characterization of the unfolding of ribonuclease A in aqueous methanol solvents. *Biochemistry.* 26:1665–1671.
4. Hirota, N., K. Mizuno, and Y. Goto. 1998. Group additive contributions to the alcohol-induced α-helix formation of melittin: implication for the mechanism of the alcohol effects on proteins. *J. Mol. Biol.* 275:365–378.
5. Sonichsen, F. D., J. E. Van Eyk, R. S. Hodges, and B. D. Sykes. 1992. Effect of trifluoroethanol on protein secondary structure: an NMR and CD study using a synthetic actin peptide. *Biochemistry.* 31:8790–8798.
6. Thomas, P. D., and K. A. Dill. 1993. Local and nonlocal interactions in globular proteins and mechanisms of alcohol denaturation. *Protein Sci.* 2:2050–2065.
7. Buck, M. 1998. Trifluoroethanol and colleagues: cosolvents come of age. Recent studies with peptides and proteins. *Q. Rev. Biophys.* 31:297–355.
8. Luidens, M. K., J. Figge, K. Breese, and S. Vajda. 1996. Predicted and trifluoroethanol-induced α-helicity of polypeptides. *Biopolymers.* 39: 367–376.
9. Martenson, R. E., J. Y. Park, and A. L. Stone. 1985. Low-ultraviolet circular dichroism spectroscopy of sequential peptides 1–63, 64–95, 96–128, and 129–168 derived from myelin basic protein of rabbit. *Biochemistry.* 24:7689–7695.
10. Blanco, F. J., M. A. Jimenez, M. Rico, J. Santoro, A. Pineda, and J. L. Nieto. 1994. NMR solution structure of the isolated N-terminal fragment of protein-G b1 domain: evidence of trifluoroethanol induced native-like β-hairpin formation. *Biochemistry.* 33:6004–6014.
11. Graf von Stosch, A., M. A. Jimenez, V. Kinzel, and J. Reed. 1995. Solvent polarity-dependent structural refolding: a CD and NMR study of a 15 residue peptide. *Proteins Struct. Funct. Genet.* 23:196–203.
12. Gast, K., D. Zirwer, M. Muller-Frohne, and G. Damaschun. 1999. Trifluoroethanol-induced conformational transitions of proteins: insights gained from the differences between α-lactalbumin and ribonuclease A. *Protein Sci.* 8:625–634.
13. Tanford, C. 1968. Protein denaturation. *Adv. Protein Chem.* 23:121–282.
14. Uversky, V. N., N. V. Narizhneva, S. O. Kirschstein, S. Winter, and G. Lober. 1997. Conformational transitions provoked by organic solvents in β-lactoglobulin: can a molten globule like intermediate be induced by the decrease in dielectric constant? *Fold. Des.* 2:163–172.
15. Hong, D. P., M. Hoshino, R. Kuboi, and Y. Goto. 1997. Clustering of fluorine-substituted alcohols as a factor responsible for their marked effects on proteins and peptides. *J. Am. Chem. Soc.* 121:8427–8433.
16. Chitra, R., and P. E. Smith. 2001. Properties of 2,2,2-trifluoroethallol and water mixtures. *J. Chem. Phys.* 114:426–435.
17. Rajan, R., and P. Balaram. 1996. A model for the interaction of trifluoroethanol with peptides and proteins. *Int. J. Pept. Protein Res.* 48:328–336.
18. Guo, H., and M. Karplus. 1994. Solvent influence on the stability of the peptide hydrogen bond: a supramolecular cooperative effect. *J. Phys. Chem.* 98:7104–7105.
19. Conio, G., E. Patrone, and S. Brighetti. 1970. The effect of aliphatic alcohols on the helix-coil transition of poly-L-ornithine and poly-L-glutamic acid. *J. Biol. Chem.* 245:3335–3340.
20. Kentsis, A., and T. R. Sosnick. 1998. Trifluoroethanol promotes helix formation by destabilizing backbone exposure: desolvation rather than native hydrogen bonding defines the kinetic pathway of dimeric coiled coil folding. *Biochemistry.* 37:14613–14622.
21. Cammers-Goodwin, A., T. J. Allen, S. L. Oslick, K. F. McClure, J. H. Lee, and D. S. Kemp. 1996. Mechanism of stabilization of helical

conformations of polypeptides by water containing trifluoroethanol. *J. Am. Chem. Soc.* 118:3082–3090.

22. Timasheff, S. N. 1970. Protein-solvent interactions and protein conformation. *Acc. Chem. Res.* 3:62–68.
23. Diaz, M. D., and S. Berger. 2001. Preferential solvation of a tetrapeptide by trifluoroethanol as studied by intermolecular NOE. *Magn. Reson. Chem.* 39:369–373.
24. Fioroni, M., M. D. Diaz, K. Berger, and S. Berger. 2002. Solvation phenomena of a tetrapeptide in water/trifluoroethanol and water/alcohol mixtures: a diffusion NMR, intermolecular NOE, and molecular dynamic study. *J. Am. Chem. Soc.* 124:7737–7744.
25. Kumar, S., K. Modig, and B. Halle. 2003. Trifluoroethanol-induced $\beta \rightarrow \alpha$ transition in β-lactoglobulin: hydration and cosolvent binding studied by ^{2}H, ^{17}O, and ^{19}F magnetic relaxation dispersion. *Biochemistry.* 42:13708–13716.
26. Gerig, J. T. 2004. Structure and solvation of melittin in 1,1,1,3,3,3-hexafluoro-2-propanol/water. *Biophys. J.* 86:3166–3175.
27. Chatterjee, C., and J. T. Gerig. 2006. Interactions of hexafluoro-2-propanol with the Trp-Cage peptide. *Biochemistry.* 45:14665–14674.
28. Roccatano, D., G. Colombo, M. Fioroni, and A. E. Mark. 2002. Mechanism by which 2,2,2-trifluoroethanol/water mixtures stabilize secondary-structure formation in peptides: a molecular dynamics study. *Proc. Natl. Acad. Sci. USA.* 99:12179–12184.
29. Roccatano, D., M. Fioroni, M. Zacharias, and G. Colombo. 2005. Effect of hexafluoroisopropanol alcohol on the structure of melittin: a molecular dynamics simulation study. *Protein Sci.* 14:2582–2589.
30. Jasanoff, A., and A. R. Fersht. 1994. Quantitative determination of helical propensities from trifluoroethanol titration curves. *Biochemistry.* 33:2129–2135.
31. Bodkin, M. J., and J. M. Goodfellow. 1996. Hydrophobic solvation in aqueous trifluoroethanol solution. *Biopolymers.* 39:43–50.
32. Nelson, R., and D. Eisenberg. 2006. Structural models of amyloid-like fibrils. *Adv. Protein Chem.* 73:235–282.
33. Westermark, P. 2005. Aspects on human amyloid foRMS and their fibril polypeptides. *FEBS J.* 272:5942–5949.
34. Ding, F., N. V. Dokholyan, S. V. Buldyrev, H. E. Stanley, and E. I. Shakhnovich. 2002. Molecular dynamics simulation of the SH3 domain aggregation suggests a generic amyloidogenesis mechanism. *J. Mol. Biol.* 324:851–857.
35. Khurana, R., J. R. Gillespie, A. Talapatra, L. J. Minert, C. Ionescu-Zanetti, I. Millett, and A. L. Fink. 2001. Partially folded intermediates as critical precursors of light chain amyloid fibrils and amorphous aggregates. *Biochemistry.* 40:3525–3535.
36. Dobson, C. M. 2002. Getting out of shape. *Nature.* 418:729–730.
37. Uversky, V. N., and A. L. Fink. 2004. Conformational constraints for amyloid fibrillation: the importance of being unfolded. *Biochim. Biophys. Acta.* 1698:131–153.
38. Ma, B., and R. Nussinov. 2002. Molecular dynamics simulations of alanine rich β-sheet oligomers: Insight into amyloid formation. *Protein Sci.* 11:2335–2350.
39. Colombo, G., I. Daidone, E. Gazit, A. Amadei, and A. Di Nola. 2005. Molecular dynamics simulation of the aggregation of the core-recognition motif of the islet amyloid polypeptide in explicit water. *Proteins.* 59:519–527.
40. Hall, C. K., and V. A. Wagoner. 2006. Computational approaches to fibril structure and formation. *Methods Enzymol.* 412:338–365.
41. Chiti, F., P. Webster, N. Taddei, A. Clark, M. Stefani, G. Ramponi, and C. M. Dobson. 1999. Designing conditions for in vitro formation of amyloid protofilaments and fibrils. *Proc. Natl. Acad. Sci. USA.* 96: 3590–3594.
42. Pallares, I., J. Vendrell, F. X. Aviles, and S. Ventura. 2004. Amyloid fibril formation by a partially structured intermediate state of α-chymotrypsin. *J. Mol. Biol.* 342:321–331.
43. Wright, H. T. 1973. Comparison of the crystal structures of chymotrypsinogen-A and α-chymotrypsin. *J. Mol. Biol.* 79:1–11.
44. Tsukada, H., and D. M. Blow. 1985. Structure of α-chymotrypsin refined at 1.68 A resolution. *J. Mol. Biol.* 184:703–711.
45. Frigerio, F., A. Coda, L. Pugliese, C. Lionetti, E. Menegatti, G. Amiconi, H. P. Schnebli, P. Ascenzi, and M. Bolognesi. 1992. Crystal and molecular structure of the bovine α-chymotrypsin-eglin c complex at 2.0 A resolution. *J. Mol. Biol.* 225:107–123.
46. Berendsen, H. J. C., J. P. M. Postma, W. F. van Gunsteren, A. Di Nola, and J. R. Haak. 1984. Molecular dynamics with coupling to an external bath. *J. Chem. Phys.* 81:3684–3690.
47. van der Spoel, D., R. van Drunen, and H. J. C. Berendsen. 1994. Groningen Machine for Chemical Simulations. Bioson Research Institute, Groningen, The Netherlands.
48. van Gunsteren, W. F., X. Daura, and A. E. Mark. 1998. GROMOS Force Field. *Encyclopedia Comput. Chem.* 2:1211–1216.
49. Berendsen, H. J. C., J. R. Grigera, and T. P. Straatsma. 1987. The missing term in effective pair potentials. *J. Phys. Chem.* 91:6269–6271.
50. Fioroni, M., K. Burger, A. E. Mark, and D. Roccatano. 2000. A New 2,2,2-Trifluoroethanol Model for Molecular Dynamics Simulations. *J. Phys. Chem. B.* 104:12347–12354.
51. Hess, B., H. Bekker, H. J. C. Berendsen, and J. G. E. M. Fraaije. 1997. LINCS: A linear constraint solver for molecular simulations. *J. Comput. Chem.* 18:1463–1472.
52. Darden, T., D. York, and L. Pedersen. 1993. Particle mesh Ewald: an Nlog(N) method for Ewald sums in large systems. *J. Chem. Phys.* 98:10089–10092.
53. Humphrey, W., A. Dalke, and K. Schulten. 1996. VMD - Visual Molecular Dynamics. *J. Mol. Graph.* 14:33–38.
54. Rezaei-Ghaleh, N., A. Ebrahim-Habibi, A. A. Moosavi-Movahedi, and M. Nemat-Gorgani. 2007. Role of electrostatic interactions in 2,2,2-trifluoroethanol-induced structural changes and aggregation of α-chymotrypsin. *Arch. Biochem. Biophys.* 457:160–169.
55. Rezaei-Ghaleh, N., A. Ebrahim-Habibi, A. A. Moosavi-Movahedi, and M. Nemat-Gorgani. 2007. Effect of polyamines on the structure, thermal stability and 2,2,2-trifluoroethanol-induced aggregation of α-chymotrypsin. *Int. J. Biol. Macromol.* 41:597–604.
56. Shimshick, E. J., and H. M. McConnel. 1972. Rotational correlation time of spin-labeled α-chymotrypsin. *Biochem. Biophys. Res. Commun.* 46:321–327.
57. Kyte, J., and R. F. Doolittle. 1982. A simple method for displaying the hydropathic character of a protein. *J. Mol. Biol.* 157:105–132.
58. Hoshino, M., Y. Hagihara, D. Hamada, M. Kataoka, and Y. Goto. 1997. Trifluoroethanol-induced conformational transition of hen egg-white lysozyme studied by small-angle X-ray scattering. *FEBS Lett.* 416:72–76.
59. Gazit, E. 2002. A possible role for π-stacking in the self-assembly of amyloid fibrils. *FASEB J.* 16:77–83.
60. Trovato, A., F. Chiti, A. Maritan, and F. Seno. 2006. Insight into the structure of amyloid fibrils from the analysis of globular proteins. *PLoS Comput. Biol.* 2:e170.
61. Warshel, A., and S. T. Russel. 1984. Calculations of electrostatic interactions in biological systems and in solutions. *Q. Rev. Biophys.* 17:283–422.
62. Affleck, R., C. A. Haynes, and D. S. Clark. 1992. Solvent dielectric effects on protein dynamics. *Proc. Natl. Acad. Sci. USA.* 89:5167–5170.